Excited-State Energy Equilibration via Subpicosecond Energy Transfer within the Inhomogeneously Broadened Light-Harvesting Antenna of LH-1-Only *Rhodobacter sphaeroides* Mutants M2192 at Room Temperature and 4.2 K

H. Matthieu Visser, Oscar J. G. Somsen, Frank van Mourik, and Rienk van Grondelle*

Department of Physics and Astronomy, Vrije Universiteit and Institute for Molecular and Biological Sciences, De Boelelaan 1081, 1081 HV Amsterdam, The Netherlands

Received: March 25, 1996; In Final Form: June 3, 1996[⊗]

Using pump−probe spectroscopy, the dynamics of energy transfer within the inhomogeneously broadened light-harvesting antenna of LH-1-only mutants of the photosynthetic bacterium *Rhodobacter sphaeroides* was studied at room temperature and 4.2 K. In both cases, the transient difference spectra shift approximately 140 cm^{-1} to lower energy, with most of the shift occurring within the first picosecond after excitation. Employing an inhomogeneous distribution for the excited-state energies of the subunits in the LH-1 antenna and using a weak coupling (Förster-type) energy-transfer mechanism, the observations can well be simulated with a transfer time between optimally overlapping antenna subunits at a single lattice distance of approximately 0.28 ps at room temperature (RT) and 0.40 ps at 4.2 K. We find that the fwhm width of the inhomogeneous distribution function decreases from 400 cm^{-1} at RT to 200 cm^{-1} at 4.2 K.

Introduction

The primary events in photosynthesis are initiated by photons absorbed in specialized light-harvesting or antenna systems. The resulting excited-state energy in the pigments of these antenna systems is rapidly transferred between many pigments before reaching a reaction center, where a sequence of fast electron-transfer steps results in stabilization of the captured energy in the form of a charge-separated state.[1] This state is used to drive further biochemical reactions, ultimately leading to the formation of ATP. In the photosynthetic bacterium *Rhodobacter (Rb.) sphaeroides* that we study in this paper, two different light-harvesting complexes are found. The photosynthetic reaction center (RC) is surrounded by a core antenna, LH-1, with peak absorption at 870 nm at room temperature. A more peripheral light-harvesting system, LH-2, absorbs at shorter wavelengths, 800 and 850 nm, and transfers its energy via the core antenna to the RC. The time it takes for an excited state in the antenna to be transferred to the RC was found to be approximately 50 ps in bacteria only containing LH-1 as an antenna system.[1,2] In several studies, it was concluded that the main factor in determining this rate is slow transfer from the antenna to the RC.[3,4,45] In this paper, we have studied the energy-transfer dynamics within the LH-1 antenna. In earlier work, from monitoring the relative quantum yield of fluorescence in chromatophores of *Rhodospirillum (Rs.) rubrum* and *Rhodopseudomenas (Rps.) capsulatus* following an intense laser pulse, it was concluded that energy transfer within the LH-1 antenna must be very fast; a hop time of 0.5−1 ps was estimated for these light-harvesting complexes.[5] In a recent paper,[6] we have shown, using transient absorption measurements on the LH-1 antenna of *Rs. rubrum* that a subpicosecond spectral evolution occurs, and this was analyzed in terms of the equilibration of excitation energy within an inhomogeneously broadened absorption band. An average hopping time between antenna subunits of 220−270 fs was estimated from this analysis. We proposed these subunits to be dimers of bacteriochlorophyll *a* (BChl*a*), with a transfer rate of 100−150 fs for optimally overlapping donor and acceptor in the light-harvesting antenna of *Rs. rubrum* at room temperature. A study in which the rate of fluorescence depolarization was measured using fluorescence up-conversion arrived at a very similar intersite hop time of about 100 fs.[7] The LH-1 antenna of the photosynthetic purple bacterium *Rb. sphaeroides* that we study in this paper has its main absorption at 880 nm at RT. It has been suggested that the width of this absorption band, 520 cm^{-1} at RT and 260 cm^{-1} at 4.2 K, arises as a large part from inhomogeneous broadening.[8] Here we show that upon excitation of the antenna fast equilibration phenomena can be observed. The speed of this process depends upon the transfer rates between the antenna subunits. We compare equilibration phenomena at RT and 4.2 K in a mutant of *Rb. sphaeroides*, containing LH-1 as its only photosynthetic pigment−protein complex.[20] Due to the absence of the reaction center, the equilibration can be studied for more than 100 ps after excitation of the antenna. At RT, a rapid establishment of a dynamic excited-state equilibrium can be expected, whereas at 4 K, where only downhill transfer is possible, excitations will be trapped in local energetic minima, leading to a "quasi-equilibrium"; that is, further equilibration takes place at exceedingly slow rates.

The LH-1 antennae of several purple bacteria, among them *Rb. sphaeroides*, can be dissociated by addition of detergent in a B820 subunit, which has been described as a dimer[9,10] of BChl*a* molecules associated with a pair of small apoproteins, α and β. These antenna subunits exhibit a further blue shift of the absorption maximum from 825 to 777 nm upon increasing the detergent concentration,[9] which is generally ascribed to the formation of monomeric BChl*a*. Both these dissociation processes can be reversed by lowering the detergent concentration, upon which reaggregation occurs.[9] It is not certain whether the reaggregated complexes have the same structure as the native complexes, but the absorption spectra are almost indistinguishable.

Unlike the LH-2 antenna of *Rps. acidophila*, for which he structure was recently resolved to a 2.5 Å resolution using X-ray diffraction,[11] the LH-1 complex has only been studied at lower resolution. A recent electron microscopy study[12] on 2-dimensional crystals of reconstituted LH-1 of *Rs. rubrum* resulted in

* Corresponding author. FAX +31-20-4447899, email rienk@nat.vu.nl.
[⊗] Abstract published in *Advance ACS Abstracts,* November 1, 1996.

S0022-3654(96)00883-0 CCC: $12.00

a 8.5 Å resolution projection map, showing a ringlike structure with inner and outer diameter of 68 and 116 Å, respectively. For this complex, 16 BChl*a* dimers were tentatively put between rings of 16 inner and 16 outer proteins. The dimer-to-dimer distance in this structure would be 17−18 Å. However, from this data, the pigment arrangement is not yet unambiguous, although it may indeed be similar to the arrangement of the B850 Chl*a*'s in LH-2. Moreover, whether these reaggregated LH-1 antenna systems indeed reflect the structure of LH-1 *in vivo* is uncertain. Boonstra et al.[13] found relatively small LH-1 complexes, with an outer diameter of 52 Å. It was suggested that these particles consist of six $\alpha\beta$ pairs with two BChl*a*'s per $\alpha\beta$ pair. These complexes, however, would be too small to contain the RC in the center of the ring. These same complexes were studied at cryogenic temperature by energy-selective fluorescence spectroscopy, and eight (dimeric) subunits were found to best describe the data.[8] Using HPLC methods, Francke and Amesz[14] recently reported a value of 24−27 BChl*a*'s per core (LH-1) antenna for seven different species and strains of purple bacteria, among them *Rb. sphaeroides*, in line with several previous studies. For example, an *in vivo* aggregation form of 12 $\alpha\beta$ protein pairs with two BChl*a* per $\alpha\beta$ pair was proposed in ref 15, in which complexes from *Rps. molischianum*, containing a RC and supposedly 12 $\alpha\beta$ pairs, were found to have an outer diameter of 107−112 Å. Meckenstock et al. purified ringlike LH-1 complexes from *Rps. marina*.[17] These complexes were found to contain six subunits in a ring structure with a diameter of 102 ± 3 Å. The subunits were supposed to contain two α and two β apoproteins and four BChl*a*'s. In all cases, these ring-shaped objects were found to be arranged in a close-packed hexagonal lattice.[16] Such lattices were also found for LH-1 complexes of the BChl*b*-containing bacteria.[18,19] Here the lattice spacing was observed to be somewhat larger, approximately 130 Å, possibly related to the fact that in these light-harvesting complexes an additional γ protein is present. An explanation for the different observed sizes for LH-1 complexes of BChl*a*-containing bacteria may be that the $\alpha\beta$ subunits can reaggregate in different forms if no RC is present. In view of the present uncertainty on the *in vivo* aggregation form, we performed energy-transfer simulations on four model structures, thus allowing some general conclusions on the dynamics of energy transfer in inhomogeneously broadened antenna systems. The structures (shown in Figure 9) are a square lattice, as was used for simplicity in most previous modeling of energy transfer in the LH-1 antenna, and the three arrangements were proposed on the basis of electron microscopy studies. Figure 9b shows hexagonal structures as proposed by for example Meckenstock et al.[17] for LH-1 of *Rps. marina*, Figure 9c shows 12 (dimeric) subunits in a ring as proposed by for example Boonstra et al.,[15] and Figure 9d shows 16 (dimeric) subunits in a ring as suggested by Karrasch et al.[12] Notice that we use the concept of "antenna subunit" in a rather loose way: it corresponds to a dimer of BChl*a* in the case of the two latter studies but to four BChl*a* molecules relatively close together in the case of the 6-ring structure proposed by Meckenstock et al.[17] We will return to this issue in the Discussion section. A preliminary report of this work was presented elsewhere.[44]

Materials and Methods

Membranes of the LH-1-only *Rb sphaeroides* mutant M2192[20] were prepared as described in for example ref 21. The data were taken with a femtosecond spectrophotometer described previously.[6] Diameters of pump and probe spots were 0.5 and 0.2 mm, respectively, and a magic-angle configuration was used.

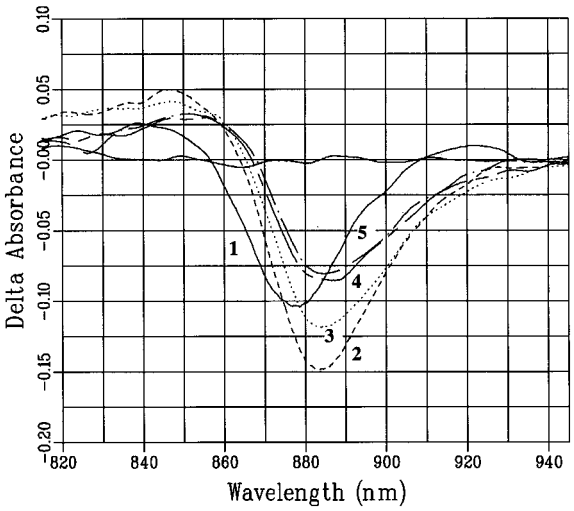

Figure 1. Transient difference spectra obtained upon Q_x (600 nm) excitation of membranes of *Rb. sphaeroides* LH-1-only mutant M2192 at room temperature (RT). Spectra 1−5 were taken with 150 fs and 1.1, 2.7, 11.0, and 17.7 ps relative delay, respectively.

The excitation pulses were centered around 600 nm, and the energy was 1.0 μJ per pulse typically, at a repetition rate of 30 Hz. The instrument response for all detection wavelengths simultaneously was obtained by measuring the induced birefringence in CS_2.[22] After proper group velocity dispersion compensation, this signal rose from 10 to 90% in 400 fs typically at all wavelengths. The signal at the central detection wavelength reached its maximum less than 100 fs earlier than the outer wavelengths, 65 nm from the center wavelength. For the measurements at 4.2 K, the sample was placed in an acrylic cuvette with 3.3 mm path length in a helium flow cryostat (Oxford Instruments CF 1204). Typically, six scans were made from short to long time delays. In every scan, typically 300 difference spectra were read out single shot and averaged at each time position. It was checked that the signal remained constant from one scan to the next. Absorption spectra of the sample were taken before and after data collection and were found to be identical.

Results

Figure 1 shows some transient difference spectra obtained on membranes of an LH-1-only mutant of *Rb. sphaeroides*, M2192, at room temperature excited with a subpicosecond laser flash around 600 nm. The maximum bleaching is 0.20. If we assume that half of this bleaching results from stimulated emission, then ground-state bleaching is approximately 10% of the total ground-state absorption. The spectra are very similar to those observed in the LH-1 antenna of *Rs. rubrum*[6] and clearly shift to lower energy with increasing delay time. The shape of the LH-1 ΔOD spectra is also similar to those observed in the isolated B820 subunits of *Rs. rubrum* (as reported in ref 6), apart from the difference in absorption maxima of these two preparations. On the high-energy side, strong excited-state absorption is present that is not observed in monomeric BChl*a* (see e.g. ref 6) and which can well be accounted for by exciton interaction in a dimer of BChl*a* molecules in a nearly parallel head-to-tail orientation (see e.g. ref 23). On the low-energy side, after relaxation from the Q_x excited state has taken place (within 200 fs[6]), stimulated emission contributes to the signal, resulting in the asymmetric S-shape observed. However, whereas in B820 no shifting of the ΔOD spectra was observed,[6] the spectra of LH-1 in Figure 1 shift approximately 140 cm^{-1} to lower energy within the first few picoseconds, from 857 to

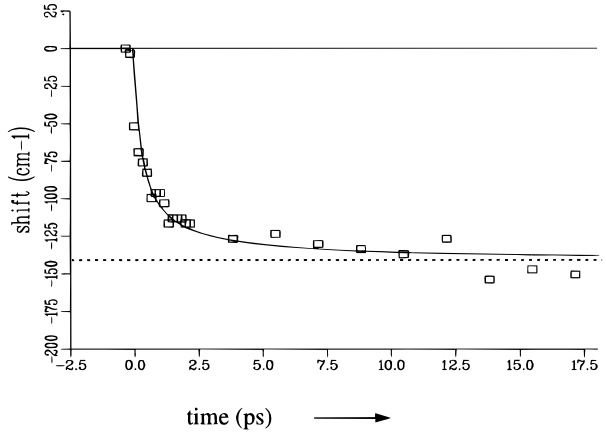

Figure 2. Shift of the transient difference spectra at RT as a function of time, measured as the shift of the zero-crossing in the spectra. The curve is the result of a simulation, using the 12-ring structure of Figure 9c ($\tau_0 = 280$ fs and $\Gamma_{IDF} = 404$ cm^{-1}). The dotted line indicates the limiting value for the shift calculated using eq 1.

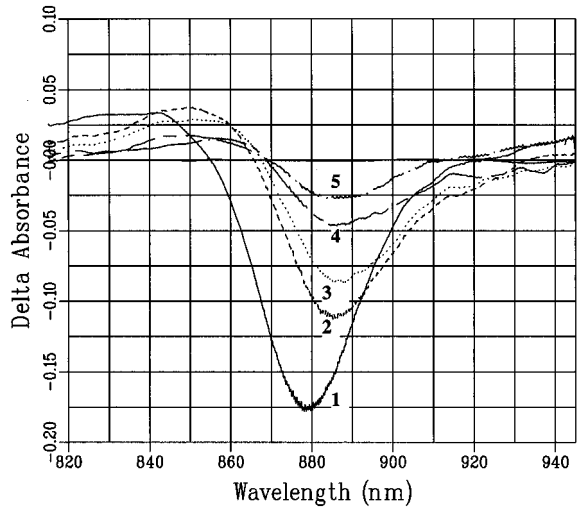

Figure 3. Transient difference spectra obtained upon Q_x excitation of membranes of *Rb. sphaeroides* LH-1-only mutant M2192 at RT, now at longer time delays. Spectra 1−5 were taken with 300 fs and 8.6, 50, 160, and 320 ps delay between excitation and detection, respectively.

869 nm as measured by the zero crossing of the difference spectra. Plotting the position of the zero crossing in the spectra as a function of delay time results in the plot in Figure 2. To get an estimate of the characteristic time constant of the equilibration process, we note that 1/e of the total shift, as detected at a delay time of 160 ps, still has to take place after ∼700 fs. Thus, the equilibration is significantly slower than observed in LH-1 complexes of *Rs. rubrum* in which the shift could be described by an exponential with 300−350 fs lifetime.[6] The line though the experimental data is the result of a simulation (next section). On a longer time scale than shown in Figures 1 and 2, a little further shifting is observed, as is evident from Figure 3. Furthermore, the spectra decrease in intensity largely due to singlet−singlet annihilation. This phenomenon will be analyzed elsewhere.[42] Similar observations were made on samples at 4.2 K. Figure 4 shows a set of transient difference spectra at 4.2 K with 0−18 ps time delay. Compared to the room temperature spectra, these spectra are about twice as narrow, like the steady-state absorption spectrum. Figure 5 again shows the shift of the spectra; the line is the result of a simulation. It is clear that both the magnitude of the shift and the rate at which the equilibration takes place are similar, but not identical, to the observations at RT. Figure 6 shows transient difference spectra at 4.2 K for time delays up

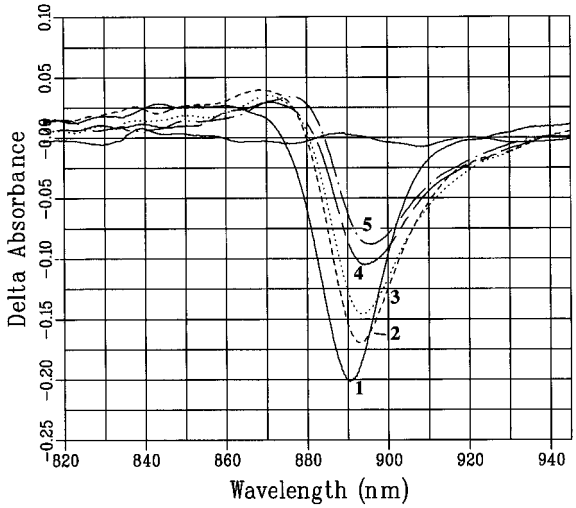

Figure 4. Transient difference spectra obtained upon Q_x excitation of membranes of *Rb. sphaeroides* LH-1 only mutant M2192 at 4.2 K. Spectra 1−5 were taken at 250 fs and 1.1, 2.0, 5.8, and 14.1 ps relative delay, respectively.

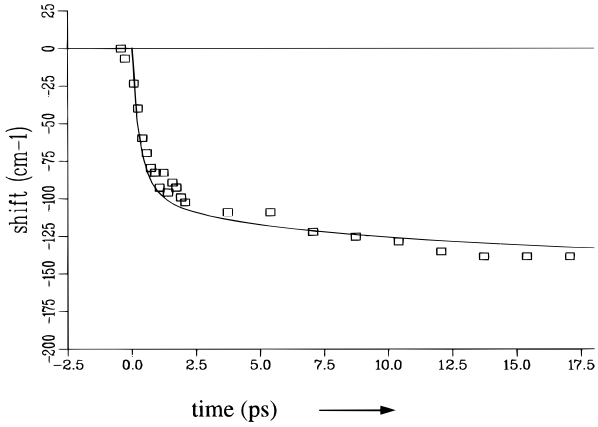

Figure 5. Shift of the transient difference spectra at 4.2 K as a function of time, measured as the shift of the zero crossing in the spectra. The curve is the result of a simulation, using the 12-ring structure of Figure 9c ($\tau_0 = 400$ fs and $\Gamma_{IDF} = 200$ cm^{-1}).

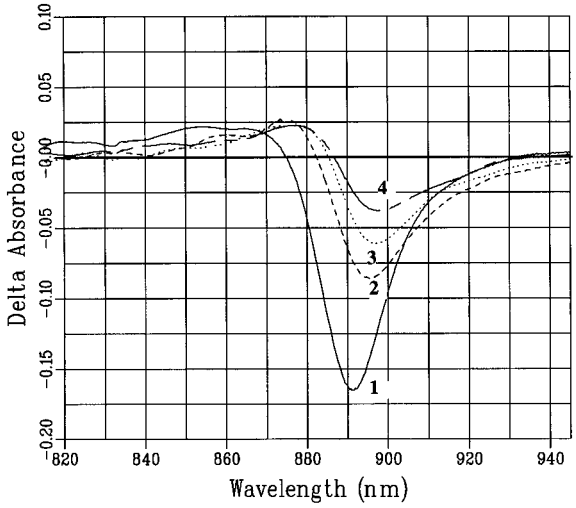

Figure 6. Transient difference spectra obtained upon Q_x excitation of membranes of *Rb. sphaeroides* LH-1-only mutant M2192 at 4.2 K, now at longer time delays. Spectra 1−4 were taken at 300 fs and 7.8, 48, and 176 ps relative delay, respectively.

to 160 ps. Upon comparison with the RT data in Figure 3, it is evident that also the annihilation phenomena at 4.2 K are very similar to the observations at RT. Finally, we notice that

between 20 and 160 ps again some additional shifting of the spectra is found.

Simulations

Steady-State Considerations. To explain the observed equilibration phenomenon, we assume that after fast $Q_x \rightarrow Q_y$ relaxation ($\tau_{ic} \lesssim 150$ fs[6]) the excitation energy distribution over the various pigments is equal to the inhomogeneous distribution function (IDF). In other words, Q_x excitation results in nonselective excitation. In principle, via up- and downhill energy transfer a Boltzmann distribution of the excitation density over *all* subunits can be reached if the width of the IDF is of similar magnitude as the thermal energy. At room temperature, this is the case: $\Gamma_{IDF} \approx 400$ cm^{-1} (fwhm), and k_BT corresponds to 210 cm^{-1}. If a Boltzmann equilibrium over all states within the IDF is reached, the equilibrium distribution can simply be calculated by multiplying the IDF with a Boltzmann factor e^{-E/k_BT}, where E is the energy of the excited state considered. For a Gaussian-shaped IDF with width Γ_{IDF} this results in a distribution that again is Gaussian with width Γ_{IDF}, but shifted toward lower energy with respect to the IDF by an amount

$$\text{shift} = \frac{\Gamma_{IDF}}{8 \ln 2} \frac{h\Gamma_{IDF}}{k_BT} \qquad (1)$$

Inserting $\Gamma_{IDF} = 400$ cm^{-1}, a reasonable number, one calculates a shift of 137 cm^{-1} at RT, close to the experimentally observed shift as shown in Figure 2. At cryogenic temperatures, however, such an approach will not work, since trapping of the excitation in some local minimum will prevent reaching a Boltzmann equilibrium within the excited-state lifetime of the antenna. This is directly obvious from considering the values of Γ_{IDF} and k_BT at 4.2 K: ~200 and 2.8 cm^{-1}, respectively. The size of the shift at 4.2 K is therefore determined by the number of subunits that can be reached via Förster energy transfer from an excited state in a local minimum (i.e., all neighboring subunits have higher excited-state energies). To give an estimate, assuming a transfer time of 100 fs for neighboring optimally matched subunits,[6] the transfer time to a neighbor n lattice spacings away is at least $n^6 \times 100$ fs. Thus, substituting $n = 4$, we find transfer between two local minima separated by four lattice distances takes at least 410 ps. Assuming for a moment a square lattice, this means that within 410 ps the lowest subunit of at most $\sim 16\pi \approx 50$ subunits can be reached. For the alternative lattice structures in Figure 9, this number scales with the 2-dimensional density ϱ of antenna subunits in the lattice and becomes ~49 for the 6-rings, ~33 for the 12-rings, and ~26 for the 16-rings packed as shown. Notice that this consideration only holds for lattices on which the energies of the pigments are not correlated with their position in the lattice; that is, there is no funnel-like organization of the antenna. Figure 7 shows the probability that a subunit at a certain energy has the lowest energy within a cluster of N subunits, randomly taken from the IDF. For $N = 12$, the average of this distribution is at $0.691\Gamma_{IDF}$ toward lower energy from the maximum of the IDF, corresponding to 138 cm^{-1} for $\Gamma_{IDF} = 200$ cm^{-1}. Similar considerations were made to explain the sharp increase in polarization of the fluorescence emission upon selective narrow-band excitation in the low-energy side of isolated LH-1 complexes of *Rb. sphaeroides* at 4.2 K.[8] Thus, assuming reasonable values for Γ_{IDF} at RT and 4 K of 400 and 200 cm^{-1}, respectively, the magnitude of the observed shift is readily explained. One can estimate that to reach the lowest of for example 50 subunits at 4 K will take at least $\sqrt{50} \approx 7$ hop times. Also, note that the shifting at 4 K will be a very multiexponetial process with time

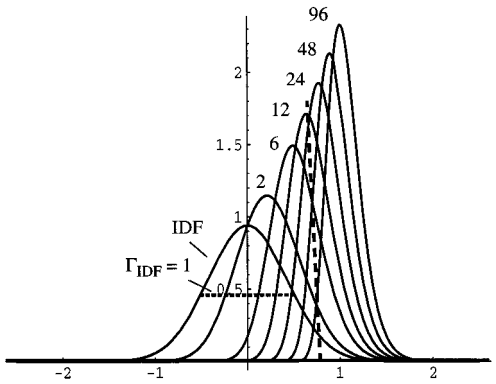

Figure 7. Probability of finding the lowest energy at a certain value in a cluster of the indicated size. The energies are normally distributed with a width 1 fwhm as shown. The vertical dashed line indicates the shift measured in the samples at 4 K 176 ps after excitation. Employing this approach, one thus finds that, 176 ps after excitation, the excitation has reached the lowest energy in a cluster of 12−24 subunits (using $\Gamma_{IDF} = 200$ cm^{-1}).

constants in the ~100 fs to >100 ps range. For a detailed analysis of the time dependence of the equilibration process we performed simulations of the dynamics as described below.

Method for Dynamic Simulations. Simulations of energy transfer within inhomogeneously broadened antenna systems were performed as described previously.[6] The homogeneous spectra were modeled by Gaussians (on an energy scale) with width Γ_{hom}(fwhm). Since the absorption spectrum should be equal to the convolution of the homogeneous spectrum with the IDF, the width of the homogeneous spectrum is fixed once a value for Γ_{IDF} is assumed.[6] The observed shift of 140 cm^{-1} at RT leads via (1) to $\Gamma_{IDF} = 400$ cm^{-1}. Since the total width of the absorption profile is 520 cm^{-1}, we find[6] $\Gamma_{hom} = 320$ cm^{-1}. These values are similar to those found for LH-1 of *Rs. rubrum*, analyzed in the same way.[6] The rate of energy transfer between two subunits at energy difference ΔE was calculated using a Förster overlap integral. Detailed balance is fulfilled if the fluorescence spectrum is shifted toward lower energy with respect to the homogeneous absorption spectrum by an amount S_t, the homogeneous Stokes shift, given by

$$S_t = \Gamma_{hom}^2/(8 \ln 2)k_BT \qquad (2)$$

This approach then results in a profile for the rate of energy transfer as a function of energy difference between donor and acceptor at RT as in Figure 8 (solid line). The profile has a width of 460 cm^{-1}, peaking at energy difference $S_t = 90$ cm^{-1}. For the simulations at 4 K, we used the homogeneous absorption spectrum proposed to explain the energy-selective fluorescence spectra of the B820 antenna subunit;[24] that is, the phonon wing (PW) as a function of wavenumber ν can be described by the function PW(ν):

$$\text{PW}(\nu) = (\nu/\gamma^2)e^{-\nu/\gamma} \qquad (3)$$

As in ref 24, we used $\gamma = 110$ cm^{-1}. The total homogeneous spectrum consists of a Lorentzian zero-phonon line (ZPL) with width γ_{ZPL} and area e^{-S} and the PW with area $(1 - e^{-S})$. Here S is the Huang−Rhys factor describing the strength of the electron−phonon coupling between chromophore(s) and protein. As in ref 24, we used $\gamma_{ZPL} = 6$ cm^{-1} and $S = 0.4$. To calculate the rate of energy transfer between two subunits, we assumed that the fluorescence spectrum of a subunit could be modeled by the mirror image of its homogeneous absorption spectrum with respect to the ZPL. Using this homogeneous spectrum, the Förster overlap integral as a function of the energy difference

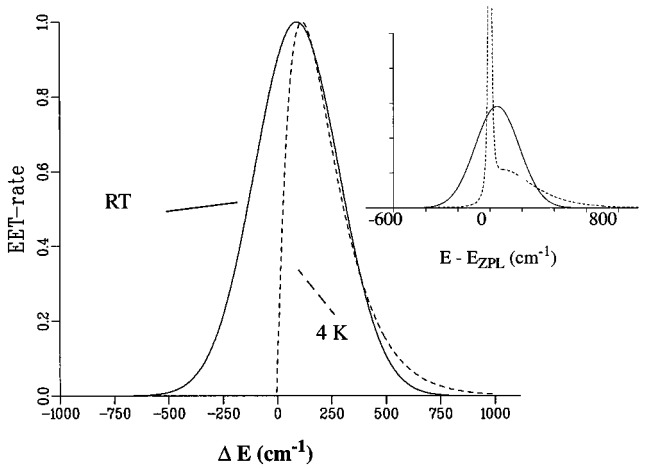

Figure 8. Energy transfer rate as a function of energy mismatch between donor and acceptor, calculated from a Förster overlap integral between absorption and emission of subunits with homogeneous absorption spectra as indicated in the inset: solid, RT, dash, 4 K. In the calculations the contribution of the zero-phonon line of the acceptor was ignored.

ΔE between two subunits can be calculated to find the rate of pairwise energy transfer as a function of the energy difference ΔE. The result is shown in Figure 8 (dashed). In this calculation we excluded the ZPL of the acceptor, since no fast relaxation from the 0−0 level is possible, a prerequisite of the Förster formula.[25] Exactly the same procedure was used recently in a simulation of energy transfer within the inhomogeneously broadened B800 band in LH-2.[26] For "uphill" energy transfer we imposed detailed balance. Both of these assumptions influence the simulated equilibration only to a minor extent as we will discuss in a next section. Both the RT and the 4 K profiles are shown normalized, so that the fastest transfer takes one unit of time. This fastest transfer time we will call the optimal hopping time τ_0. Upon comparison of the two calculated profiles, it is clear that the "downhill" shapes of the RT and the 4 K profile are very similar, but in contrast to the situation at RT, "uphill" energy transfer is virtually impossible at 4 K.

In the simulations, optimally packed 12-rings were used, as well as square and hexagonal lattices as in Figure 9. Also, 16-rings packed in a hexagonal lattice as in Figure 9d were used. Transfer to subunits more than a single lattice distance away was included by inserting a r^{-6} dependence of the transfer rate between donor and acceptor at distance r. Periodic boundary conditions to avoid edge effects were included unless specified otherwise. When the periodic boundary conditions are switched off, the simulations show the equilibration in single or a few clustered 6- or 12-rings. To simulate larger systems, lattices with approximately 100 subunits were used: 3 × 3 12-rings, 4 × 4 6-rings, 3 × 3 16-rings, or 10 × 10 subunits in a square lattice. Periodic boundary conditions were then applied to each of these structures. The rate equations that describe the equilibration were integrated numerically. The calculation was repeated 512 times for large systems (∼100 subunits) and 8192 times for small systems (∼12 subunits), and for each run the excited-state energies of the subunits were randomly taken from the IDF. These results were averaged. The standard deviation in the simulations after these averages is less than 2% of the maximum shift typically. The influence of the periodic boundary conditions on the simulated equilibration will be discussed in a later section.

Results of the Simulations. *Room Temperature*. The full line through the data points in Figure 2 is the result from a

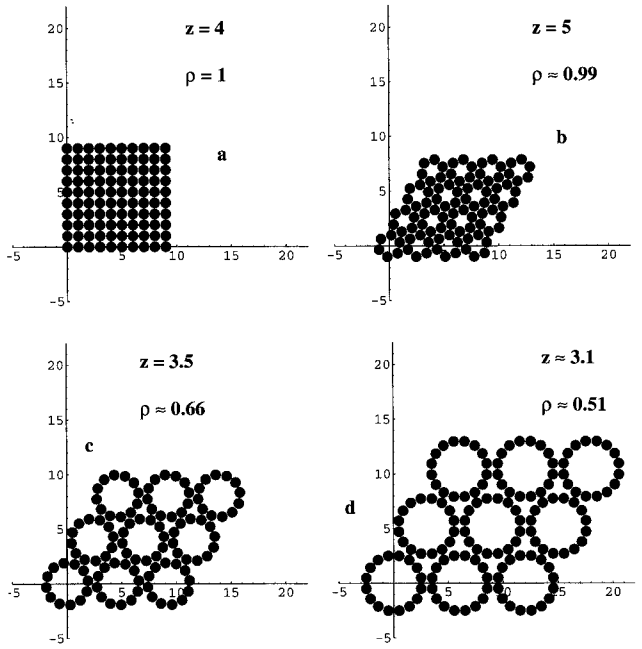

Figure 9. Structures used for the 2-dimensional lattice in the simulations. Distance between nearest neighbors is 1. Z indicates the average number of neighbors, and ϱ the 2-dimensional density for infinite lattices build up by repeating the structure shown in two directions.

simulation using 3 × 3 12-rings at RT. Input parameters are $\Gamma_{IDF} = 404$ cm^{-1} and $\tau_0 = 280$ fs. The dotted line indicates the limiting value for the shift at room temperature, using (1). The fit is satisfactory for the 0−18 ps time domain. Thus, combination of reasonable energetic parameters Γ_{IDF} (and thereby Γ_{hom}) with a plausible structure for the LH-1 antenna results in a satisfactory description of the equilibration process at RT. However (as shown in Figure 11, discussed below), the equilibration process simulated in the other structures shown in Figure 9 is very similar, and none of the proposed lattice structures can be excluded on basis of the observed equilibration dynamics.

4 K. The line in Figure 5 is the result of a simulation using 3 × 3 12-rings at 4.2 K. Here, the input parameters are $\tau_0 =$ 400 fs and $\Gamma_{IDF} = 200$ cm^{-1}. Notice that for 108 connected subunits the steady-state considerations of Figure 7 predict a significant further shift than observed in Figure 5. A simulation (again using 3 × 3 12-rings and $\Gamma_{IDF} = 200$ cm^{-1}, not shown) running for times up to 40 000 τ_0 (corresponding to 16 ns for $\tau_0 = 400$ fs) gave a final shift of 209 cm^{-1}, close to the statistical limit (Figure 7) of 1.08 $\Gamma_{IDF} = 215$ cm^{-1}. However, the last phase in the equilibrium is very slow. At 400 τ_0 (160 ps for τ_0 = 400 fs) the shift is only 161 cm^{-1}, to be compared with the experimental value of 154 cm^{-1} at 160 ps. In the 12-ring structure, the statistical limit is reached more slowly than in packed 6-rings and in square lattices, where both connectivity and density of the subunits are higher, thereby decreasing trapping in local minima.

Switching Off the Periodic Boundary Conditions; Studying Small Complexes. By switching off the periodic boundary conditions in the simulations, equilibration in isolated rings can be simulated, or in small clusters of these. The effect on the rate of equilibration is quite significant, as is shown in Figure 10. Here, the simulated equilibration at room temperature in single 12-rings is compared to the equilibration of one 12-ring, connected to identical copies (solid and dashed curve, respectively). Since the coordination number in single 12-rings is only 2, whereas it is 3.5 in 12-rings packed as in Figure 9,

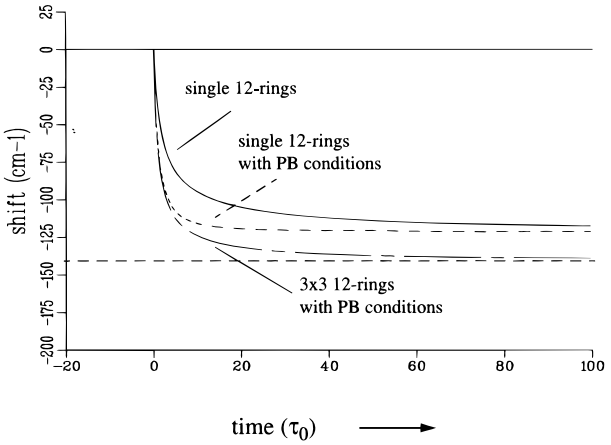

Figure 10. Equilibration at RT simulated in single 12-rings (solid) and connected to identical copies by periodic boundary conditions in a lattice as in Figure 9 (dashed). Also shown is the simulated equilibration in 3 × 3 12-rings connected by periodic boundary conditions, simulating a large system. The horizontal dashed line indicates the shift calculated by eq 1. Input parameter was $\Gamma_{IDF} = 404$ cm^{-1}, as in Figure 2. τ_0 is the transfer time between optimally overlapping donor and acceptor.

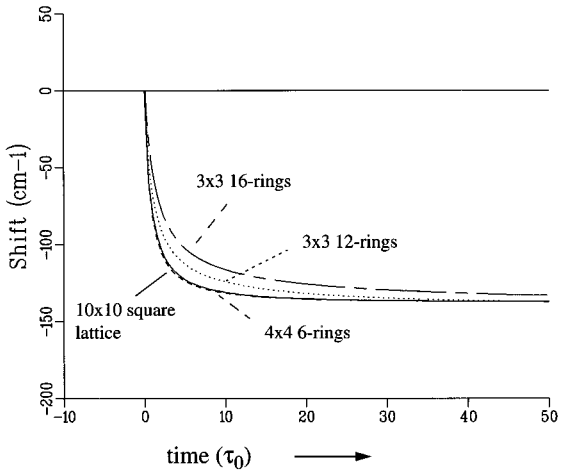

Figure 11. Simulated equilibration in the four lattice structures in Figure 9: solid, 10 × 10 subunits on square lattice; dashed, 4 × 4 6-rings; dotted, 3 × 3 12-rings; chain-dashed, 3 × 3 16-rings. Input parameter was $\Gamma_{IDF} = 404$ cm^{-1}.

equilibration in single rings is slower than in connected rings. The size of the shift in these simulations is limited by the number of subunits taken from the IDF. This is clear from comparison with the chain-dashed line, showing the result for 3 × 3 12-rings with periodic boundary conditions. Now the limit predicted by eq 1 (indicated by the dashed line) is reached. Further increase in the number of connected subunits did not change the simulated equilibration.

Comparing Simulations in Different Lattices. Figure 11 shows the effect of a particular lattice structure on the simulated equilibration at RT. The input parameter, as in Figure 2, was $\Gamma_{IDF} = 404$ cm^{-1}. The dotted line was obtained by performing the simulation on 3 × 3 12-rings, the solid line using 10 × 10 subunits in a square lattice, the dashed line using 4 × 4 6-rings, and the chain-dashed line using 3 × 3 16-rings, connected as in Figure 9. The initial phase in all four curves is similar, but in the 12-rings a slower phase arises most likely from the lower density and average coordination number of this lattice structure. This effect is even stronger in the 16-ring structure (chain-dashed line). Putting $\tau_0 = 280$ fs, the dotted line in Figure 11 becomes the fit in Figure 2. For simulations at 4.2 K, similar observations of the influence of the lattice structure on the equilibration were made (not shown).

Discussion

The equilibration phenomena that we observe in the LH-1 antenna of photosynthetic purple bacteria are well explained by the combination of subpicosecond energy transfer and inhomogeneous broadening in these complexes. Subpicosecond energy transfer was predicted on basis of the intensity dependence of the antenna fluorescence of chromatophores of *Rs. rubrum* and *Rps. capsulatus*.[5] Most direct evidence came from subpicosecond depolarization of transient absorption data.[28] Fluorescence depolarization was recently observed on a subpicosecond time scale using up-conversion.[7] In this work, the fluorescence anisotropy from M2192 membranes was found to decay with time constants of approximately 110 and 400 fs. These data could be simulated with an optimal hopping time τ_0 of 80 and 265 fs for rings consisting of 8 and 16 "sites", respectively. The intermediate value of ∼160 fs is faster than our estimate $\tau_0 = 280$ fs for 12-rings, but note that in the modeling we present here, we explicitly assume additional fast energy transfer between different rings, in contrast to ref 7. Modeling the observed red shift using isolated (as in ref 7) 12-rings would result in a ∼1.7 times shorter τ_0, i.e., $\tau_0 = 165$ fs, as can be seen from Figure 10. Thus, both data sets can be modeled using essentially the same parameters, and the issue that remains is whether energy transfer between rings is as fast as assumed in our modeling. The observed close packing of LH-1 complexes in electron microscopy of LH-1 membranes of *Rps. marina*[16] suggests fast inter-ring transfer, and so does the observation of large domains for annihilation at RT.[5] From the projection maps by Karrasch et al.,[12] an inter-ring dimer-to-dimer distance of 21 Å can be estimated, somewhat larger than the 17−18 Å intra-ring dimer-to-dimer distance. Moreover, in our modeling we have neglected the orientation factor κ^2, thus possibly overestimating the rate of transfer between neighboring rings by a factor of ∼4 in the case that the BChl*a* transition dipole moments are aligned along the tangent of the ring. Future modeling may therefore be aimed at the intermediate situation where transfer within rings is ∼4 times faster than between rings. The aforementioned study[7] also found evidence for fast, 0.5−1 ps, singlet−singlet annihilation, similar to the observations described here. Moreover, the ∼0.7 ps time constant describing the red-shift of the transient absorption spectra directly suggests a situation where this annihilation process is limited by energy transfer. The localization of the excited-state energy on the red side of the IDF will increase the efficiency of subsequent s−s annihilation, in full agreement with the notions in ref 7. Thus, the model presented here *directly* leads to a separation of time scales with fast equilibration followed by slower annihilation. This result is not at all obvious in a model assuming a completely delocalized exciton state for LH-1.

The value for τ_0 is slower than the value estimated in our previous work describing similar phenomena in the LH-1 antenna of *Rs. rubrum*, but the value for Γ_{IDF} is very similar. In this previous study,[6] we found $\Gamma_{IDF} = 414$ cm^{-1} and $\tau_0 =$ 100−150 fs. The fact that the equilibration in LH-1 is ∼2.5 times slower in *Rb. sphaeroides* than in *Rs. rubrum* may be the result of a slightly different structure of the two complexes. With the r^{-6} dependence of the Förster mechanism employed, the subunit−subunit distance needs to be only 17% larger to account for such an effect. We remind that the *Rs. rubrum* Q_y absorption is almost 10 nm red shift with respect to the *Rb. sphaeroides* absorption spectrum, which must originate from

some structural difference. It was recently found[47] that in LH-2 of *Rs. molischianum* the Mg-to-Mg distance within the B850 heterodimer is 9.2 Å, while this distance is 8.9 Å for BChl*a*'s on neighboring dimers. Thus, the BChl's in LH-2 of *Rs. molischianum* are more evenly distributed over the ring than in *Rs. acidophila*, where these values were earlier reported[11] to be 8.7 and 9.7 Å, respectively. It cannot be excluded from present structural studies that similar differences are present in LH-1 of different bacteria as well.

The number of subunits over which the equilibration density equilibrates at 4 K, that we estimate at 12−24 from Figure 7 (using $\Gamma_{IDF} = 200$ cm^{-1} and the observed shift of 140 cm^{-1}), is somewhat lower than the domain size estimated from annihilation experiments[29] on chromatophores of *Rs. rubrum*. These data were analyzed in terms of a two-pool model, with BChla_{880} and BChla_{896}. At RT, >1000 BChl*a*'s were found connected by means of energy transfer. At 4 K, a domain size of 35−75 BChla_{880}'s was found. Since the analysis of these measurements did not include any spectral inhomogeneity, the hop times found from these annihilation studies (0.5−1 ps at RT, 2.0−3.3 ps at 4 K) cannot be directly compared to the values for τ_0 we find here. However, it is interesting that the analysis of these annihilation measurements also arrives at a slow increase of the pairwise transfer time upon cooling from RT to 4 K. In the simulations presented here, the values for S and γ are identical to the values used to describe energy-selective spectroscopy on the isolated antenna subunit B820,[24] but in contrast to this paper we use a temperature-dependent IDF. This implies that the IDF consists of a static part and a part that is dynamic in the sense that it is temperature-induced. However, the time scale of these dynamics most likely is much slower than that of energy transfer in this antenna system. A temperature-dependent width of the IDF was also found in an analysis of the hole-burned spectra of rhodopsin and bacteriorhodopsin.[30] In this study, the fwhm width of the Gaussian IDF increased by a factor of 2.5 upon raising the temperature from 1.5 K to RT, similar to our findings. The IDF widths are 700 and 470 cm^{-1} at 1.5 K for rhodopsin and bacteriorhodopsin, respectively. At RT, these values are 1800 and 1100 cm^{-1}, respectively.

Several studies[31,32] find evidence for excitonic states in LH-1. The question is, what is the effective number of coupled pigments, the "delocalization length", or "degree of localization" (as defined in e.g. ref 33)? For LH-2 of *Rps. acidophila*, a center-to-center distance of 8.7 Å is found for BChla_{850} belonging to the same $\alpha\beta$ pair and 9.7 Å for BChla_{850}'s belonging to neighboring $\alpha\beta$-pairs.[11] The difference between *intra*- and *inter*dimer distances is small, but it may be sufficient to result in an effectively dimeric character of the antenna subunit in LH-2. Within dimers, orbital overlap may lead to strong exchange interaction. Between dimers, the interaction may be significantly weaker due to the exponential falloff of the exchange interaction.[34] From the shape of the transient difference spectrum, Pullerits et al.[35] estimate a delocalization length of 4 ± 2 for LH-2. Although the ring in LH-1 is somewhat larger, the experimental difference spectra are similar, and the result may be approximately valid for LH-1 as well. However, the femtosecond depolarization experiments on LH-1[7] are very well explained by assuming excitation hopping between BChl*a* dimers. Moreover, in LH-1 the intra- and interdimer distance seem more distinguishable in the structure by Karrasch et al.[12] than in LH-2. Actually, the estimated 17−18 Å dimer-to-dimer distance in this proposed LH-1 structure is rather close to the 21 Å BChla_{800}−BChla_{800} distance in LH-2. Transfer between these pigments was modeled[26] within a framework as described here, using incoherent Förster energy transfer between monomeric BChla_{800} molecules. Previously, there has been substantial biochemical evidence that the LH-1 antenna can be thought of as being built up from subunits $\alpha\beta$-BChla_2[9,10] or possibly further assembled into tetramers ($\alpha\beta$-BChl$a_2)_2$,[11] but see also ref 43. Furthermore, both the T-S[10] and the excited-state difference spectra[6] of LH-1 and the B820 subunit are very similar and clearly different from monomeric BChl*a*, strongly suggesting that the basic antenna subunit in LH-1 is a BChl*a* dimer. On the basis of this evidence, we favor interpretation of the observed equilibration in LH-1 of *Rb. sphaeroides* as being due to an incoherent hopping among weakly coupled dimers that have an inhomogeneous energy distribution of width Γ_{IDF}. However, we note that in case of stronger coupling effectively leading to tetrameric subunits, the data reported here can be equally well modeled using a hexagonal arrangement of such subunits as in Figure 9b and the same value for Γ_{IDF}. Therefore, the conclusion from the comparison of experimental data and simulations must be that the experiment is yielding well-defined values for the inhomogeneous broadening bandwidth Γ_{IDF} and the optimal intersubunit hop time τ_0 but is less sensitive to the delocalization length. Other experiments which determine the oscillator strength of the LH-1 Q_y transition should shed light on this issue. For LH-2 of *Chromatium tepidum*, it was recently concluded that the B850 oscillator strength is approximately 4 times that of the (monomeric BChla) B800 band.[48] Upon increasing delocalization of the excited state over more than ∼4 Chl's, the point-dipole approximation that we used here for deriving the rate between subunits will become less appropriate, and other models for the excited-state dynamics should be applied. However, our present view is that the degree of inhomogeneous and homogoneous broadening is not allowing for such a large degree of delocalization.

Limitations of the Model in the Simulations. The profile in Figure 8, showing the energy transfer rate as a function of the energy mismatch between donor and acceptor at one lattice distance, was calculated using the overlap function between donor fluorescence and acceptor absorption as in ref 25. In the 4 K simulations, the fluorescence spectrum of the donor was put equal to the mirror image of its absorption profile with respect to the 0−0 transition. With no fast relaxation channels available from the 0−0 transition in the acceptor, we did not include this 0−0 line in the calculated overlap integral. However, as the width of the ZPL (a few cm^{-1} at most) is negligible compared with the width of both the phonon wing and the IDF, including this 0−0 line in the overlap integral in the 4 K simulations does not alter the simulated equilibration significantly. At RT, the ZPL has broadened due to dephasing, and its contribution to the homogeneous spectrum is negligible due to the thermal population of higher phonon levels (see e.g. ref 24). It has been suggested[36,37] that the homogeneous spectrum can well be modeled by a Gaussian line shape at RT, as we did in the simulations presented. The value of Γ_{IDF}, ∼400 cm^{-1} at RT, leads to reasonable values for both Γ_{hom} and the homogeneous Stokes shift S_t: 323 and 90 cm^{-1}, corresponding to 24 and 7 nm, respectively. Thus, we feel that the transfer functions at RT and 4 K depicted in Figure 8 are at least reasonable approximations. Not included in the simulations is the orientation factor κ^2 taking into account the relative orientation of donor and acceptor transition dipole moments.[25,45] To include this factor, more structural knowledge on the LH-1 complex is needed. The influence of κ^2 on the energy equilibration in LH-1 was studied in ref 36. However, for a C-12 (or C-16) symmetric ring structure, the value of κ^2 is the

same for all neighboring subunits in one ring and therefore is included in the value for τ_0. Between rings, κ^2 can have any value in principle (depending on the lattice structure), but if we take a LH-2 as an example for LH-1, then it is seen that *within* the ring κ^2 is close to the maximum value of 4 for neighboring dimers and approximately 1 for neighboring dimers from different rings. Finally, we did not include the vibronic contributions to the homogeneous spectrum. The main effect of including these into the calculation would be a tail on the high-energy side of the profile for the rate of energy transfer as a function of the energy gap between donor and acceptor as shown in Figure 8. However, the fluorescence spectrum of the antenna subunit, B820, does not show strong vibrational bands[24,46] that would have altered the calculated profile to such an extent that the simulated equilibration would have been significantly different.

RT Data. The time-dependent shifting of the spectra between 0 and 18 ps (Figure 2) is well described with the model. As Figure 11 shows, the dependence on the exact lattice structure is rather weak, thus allowing a reasonable estimate of the optimal hopping time τ_0. A minor further shifting of the spectra between 20 and 320 ps cannot be accounted for in the simulations. Using a slightly larger Γ_{IDF} would lead to a larger shift, but in the simulations the full shift takes place within $100\tau_0$, or ~20 ps. An extension of the simulation, assuming large domains (for example, a few 12-rings) with relatively fast transfer *within* domains (of one or more rings) and slow transfer *between* them, may explain the observed slower phase in equilibration at RT. Such suggestions were made previously to explain the anisotropy decay in LH-1 from 0.1 to a very low value between one and several tens of picoseconds.[27] The main features of the observed equilibration however are readily explained by the model simulations applied on large (~100 subunits) domains connected with periodic boundary conditions, using $\Gamma_{IDF} = 404$ cm^{-1} and $\tau_0 = 280$ fs.

4 K Data. At 4.2 K, the equilibration in the first 18 ps is reasonably described by the model simulations, using $\tau_0 = 400$ fs and $\Gamma_{IDF} = 200$ cm^{-1}, as is evident from Figure 5. Whereas the simulations predict a further shift from 135 to 161 cm^{-1} between 20 and 160 ps (using $\tau_0 = 400$ fs and the 12-ring structure), a somewhat smaller shift is observed experimentally, from 138 to 154 cm^{-1}. Slower transfer between rings may again be the origin of this observation.

Comparison of the experimentally observed shift of 154 cm^{-1} at 160 ps with the steady-state consideration shown in Figure 7 suggests that the lowest of 12−24 subunits is reached. Again, the main features of the experimentally observed shift are well described in these simulations. In our view, further modeling should await more detailed structural data on these LH-1 complexes.

General Remarks. Although experimentally the observed equilibration is similar (compare Figures 2 and 5), the nature of the equilibrium state at RT is very different from the frozen quasi-equilibrium of locally trapped states at 4 K. In a previous study,[6] we have shown that at RT, after equilibration the majority of transfer times between neighboring subunits is still less than a picosecond, thus creating a dynamic equilibrium. At 4 K, the situation is very different with essentially "downhill" energy transfer only. Therefore, excitations get locally trapped at an energy in the IDF that is mainly determined by the distance dependence of the energy-transfer mechanism. In some papers, this energy is called the "localization energy".[38] Local trapping probably contributes to the strong temperature dependence of the fluorescence quantum yield of LH-1 in *Rs. rubrum* chromatophores.[39] Upon lowering the temperature from RT to 4.2 K, the fluorescence was found to increase by a factor of 4. In contrast to the explanation in ref 39, where the effect was ascribed to a general decrease of the Förster overlap integral between antenna fluorescence and RC absorption with lowering of the temperature, it now seems likely that at least part of this effect is caused by excitations that were locally trapped in the antenna and therefore can no longer reach the reaction centre.

As was already indicated in ref 8, Figure 7 may also be used to explain the hole-burning data reported previously on LH-1: only if the lowest-energy subunit of a cluster is excited, a narrow hole can be burnt. Therefore, in a first approximation Figure 7 shows the action profile as measured by Reddy et al.[32] Using again $\Gamma_{IDF} = 200$ cm^{-1} and taking an effective domain size of 12, we find that the action profile should peak at 128 cm^{-1} lower energy than the main absorption maximum (at 4.2 K 11 261 cm^{-1}, 888 nm, so the profile in this approximation would peak at 11 133 cm^{-1}, 898 nm) and have a width 108 cm^{-1} (fwhm). These values are similar to the observations,[32] finding a profile peaking at 11 169 cm^{-1}, 895.3 nm, and a width (fwhm) of approximately 150 cm^{-1}. Thus, modeling the light-harvesting antenna as a 2-dimensional array of subunits that are inhomogeneously distributed in energy and connected by fast energy transfer as we do here, one arrives at a different explanation for the observed action profile. No special exciton band (B896) is needed; rather, the profile originates from locally trapped excited states in the low-energy side of the absorption band. The broad profile associated with the narrow hole would correspond to the phonon wing. In the profile in Figure 8, this gives rise to a width of approximately 330 cm^{-1}. The spectra obtained by burning on the low-energy side in the LH-1 absorption of *Rb. sphaeroides* are ~400 cm^{-1} wide.[32]

It is of interest that a very similar approach of energy transfer between molecules inhomogeneously distributed in energy has been used to describe (sub)picosecond energy relaxation in conjugated polymers at RT,[40] as well as triplet energy transfer taking place over several milliseconds in glassy benzophenone at cryogenic temperatures.[41] The width of the IDF was 514 cm^{-1} in conjugated polymers at RT and 612 cm^{-1} in glassy benzophenone at cryogenic temperatures. Residence times of $\lesssim$250 fs and 10 ns were found in these two studies, respectively. Thus, the concept of dispersive energy transfer has also been successfully applied to energy transfer via the exchange mechanism and over a wider range of orders in time than in this study and appears of general relevance for energetically disordered systems.

In conclusion, a model with an inhomogeneous distribution of energies for subunits that transfer energy via a Förster energy transfer mechanism explains the main features of observed subpicosecond equilibration in LH-1 complexes at room temperature and at 4.2 K accurately. In addition, the model allows to understand several other spectroscopic data on similar light-harvesting systems as well.

Acknowledgment. This research was supported by the Netherlands' Organization for Research (N.W.O.) through the Foundation of Life Sciences (S.L.W.) and through EC Contracts CT 92 0796 and CT 93 0278. Dr. M. Du assisted in early test experiments and was able to visit the Amsterdam laboratory with a traveling grant from Bio Centrum Amsterdam. The M2192 preparations were kindly provided by Prof. dr. C. N. Hunter, University of Sheffield (UK). Finally, we acknowledge stimulating discussions with Dr. T. Pullerits (Lund University, Sweden).

References and Notes

(1) Van Grondelle, R.; Dekker, J. P.; Gillbro, T.; Sundström, V. *Biochim. Biophys. Acta* **1994**, *1187*, 1.

(2) Nuijs, A. M.; Van Grondelle, R.; Joppe, H. P. L.; Van Bochove, A. C.; Duysens, L. N. M. *Biochim. Biophys. Acta* **1985**, *723*, 30. See also the low-intensity study by: Sundström, V.; Van Grondelle, R.; Bergström, H.; Äkeson, E.; Gilbro, T. *Biochim. Biophys. Acta* **1985**, *851*, 431.

(3) Timpmann, K.; Zhang, F. G.; Freiberg, A.; Sundström, V. *Biochim. Biophys. Acta* **1993**, *1183*, 185.

(4) Beekman, L. M. B.; Van Mourik, F.; Jones, M. R.; Visser, H. M.; Van Grondelle, R. *Biochemistry* **1994**, *33*, 3143.

(5) Bakker, J. G. C.; Van Grondelle, R.; Den Hollander, W. Th. F. *Biochim. Biophys. Acta* **1983**, *725*, 508.

(6) Visser, H. M.; Somsen, O. J. G.; Van Mourik, F.; Van Stokkum, I. H. M.; Van Grondelle, R. *Biophys. J.* **1995**, *69*, 1083.

(7) Bradforth, S. E.; Jimenez, R.; Van Mourik, F.; Van Grondelle, R.; Fleming, G. R. *J. Phys. Chem.* **1995**, *99*, 16179.

(8) Van Mourik, F.; Visschers, R. W.; Van Grondelle, R. *Chem. Phys. Lett.* **1992**, *195*, 1.

(9) Visschers, R. W.; Chang, M. C.; Van Mourik, F.; Parkes-Loach, P. S.; Heller, B. A.; Loach, P. A.; Van Grondelle, R. *Biochemistry* **1991**, *30*, 2951.

(10) Van Mourik, F.; Van der Oord, C. J. R.; Visscher, K. J.; Parkes-Loach, P. S.; Loach, P. A.; Visschers, R. W.; Van Grondelle, R. *Biochim. Biophys. Acta* **1991**, *1059*, 111.

(11) Mc Dermott, G.; Prince, S. M.; Freer, A. A.; Hawthornthwaite-Lawless, A. M.; Papiz, M. Z.; Cogdell, R. J.; Isaacs, N. W. *Nature* **1995**, *374*, 517.

(12) Karrasch, S.; Bullough, P. A.; Ghosh, R. *EMBO J.* **1995**, *14*, 631.

(13) Boonstra, A. F.; Visschers, R. W.; Calkoen, F.; Van Grondelle, R.; Van Bruggen, E. F. J.; Boekema, E. J. *Biochim. Biophys. Acta* **1992**, *1142*, 181.

(14) Francke, C.; Amesz, J. *Photosynth. Res.* **1995**, *46*, 347.

(15) Boonstra, A. F.; Germeroth, L.; Boekema, E. J. *Biochim. Biophys. Acta* **1994**, *1184*, 227.

(16) Meckenstock, R. U.; Krusche, K.; Brunisholz, R. A.; Zuber, H. *FEBS Lett.* **1992**, *311*, 135.

(17) Meckenstock, R. U.; Brunisholz, R. A.; Zuber, H. *FEBS Lett.* **1992**, *311*, 128.

(18) Stark, W.; Kühlbrandt, W.; Wildhaber, I.; Wehrli, E.; Mühlethaler, K. *EMBO J.* **1983**, *3*, 777.

(19) Engelhardt, H.; Baumeister, W.; Saxton, W. O. *Arch. Microbiol.* **1983**, 169.

(20) Hunter, C. N.; Van Grondelle, R.; Van Dorsen, R. J. *Biochim. Biophys. Acta* **1989**, *973*, 383.

(21) Visschers, R. W.; Nunn, R.; Calkoen, F.; Van Mourik, F.; Hunter, C. N.; Rice, D. W.; Van Grondelle, R. *Biochim. Biophys. Acta* **1989**, *1100*, 259.

(22) Greene, B. J.; Farrow, R. C. *Chem. Phys. Lett.* **1983**, *98*, 273.

(23) Schelvis, J. P. M.; Aartsma, T. J. *Chem. Phys.* **1995**, *194*, 303.

(24) Pullerits, T.; Monshouwer, R.; Van Mourik, F.; Van Grondelle, R. *Chem. Phys.* **1995**, *194*, 395.

(25) Förster, Th. In *Modern Quantum Chemistry*; Sinanoglu, O., Ed.; Academic Press: New York, 1965; Vol. III, p 93.

(26) Hess, S.; Åkesson, E.; Cogdell, R. J.; Pullerits, T.; Sundström, V. *Biophys. J.* **1995**, *69*, 2211.

(27) Hunter, C. N.; Van Grondelle, R.; Olsen, J. D. *TIBS* **1989**, *14*, 71.

(28) Sundström, V.; Van Grondelle, R.; Bergström, H.; Åkesson, E.; Gillbro, T. *Biochim. Biophys. Acta* **1986**, *851*, 431.

(29) Deinum, G.; Aartsma, T. J.; Van Grondelle, R.; Amesz, J. *Biochim. Biophys. Acta* **1989**, *976*, 63.

(30) Loppnow, G. R.; Mathies, R. A.; Middendorf, T. R.; Gottfried, D. S.; Boxer, S. G. *J. Phys. Chem.* **1992**, *96*, 737.

(31) Dracheva, T. V.; Novoderzhkin, V. I.; Razjivin, A. P. *Chem. Phys.* **1995**, *194*, 223.

(32) Reddy, N. R. S.; Picorel, R.; Small, G. J. *J. Phys. Chem.* **1992**, *96*, 6458.

(33) Fidder, H.; Knoester, J.; Wiersma, D. A. *J. Chem. Phys.* **1991**, *95*, 7880.

(34) Dexter, D. L. *J. Chem. Phys.* **1953**, *21*, 836.

(35) Pullerits, T.; Chachisvilis, M.; Sundström, V. *Photosynthesis: from Light to Biosphere*; Mathis, P., Ed.; Kluwer Academic Publishers: Dordrecht, 1995; Vol. I, p 107.

(36) Pullerits, T.; Visscher, K. J.; Hess, S.; Sundström, V.; Freiberg, A.; Timpmann, K.; Van Grondelle, R. *Biophys. J.* **1994**, *66*, 236.

(37) Rebane, K. K. *Impurity Spectra of Solids*; Plenum Press: New York, 1970.

(38) Bässler, H.; Deussen, M.; Heun, S.; Lemmer, U.; Mahrt, R. F. *Z. Phys. Chem. (Munich)* **1994**, *184*, 233.

(39) Rijgersberg, C. P.; Van Grondelle, R.; Amesz, J. *Biochim. Biophys. Acta* **1980**, *592*, 53.

(40) Kersting, R.; Lemmer, U.; Mahrt, R. F.; Leo, K.; Kurz, H.; Bässler, H.; Göbel, E. O. *Phys. Rev. Lett.* **1994**, *70*, 3820.

(41) Richert, R.; Bässler, H.; Ries, B.; Movaghar, B.; Grünewald, M. *Philos. Mag. Lett.* **1989**, *59*, 95.

(42) Visser, H. M.; Somsen, O. J. G.; Valkunas, L.; Van Grondelle, R. Manuscript in preparation.

(43) Van Mourik, F.; Corten, E. P. M.; Van Stokkum, I. H. M.; Visschers, R. W.; Visscher, K. J.; Kraayenhof, R.; Van Grondelle, R. *Research in Photosynthesis*; Kluwer Academic Publishers: Dordrecht, 1992; p 1.101-1-4.

(44) Visser, H. M.; Somsen, O. J. G.; Van Mourik, F.; Van Grondelle, R. In *Photosynthesis: from Light to Biosphere*; Mathis, P., Ed.; Kluwer Academic Publishers: Dordrecht, 1995; Vol. I, p 343.

(45) Somsen, O. J. G.; Valkunas, L.; Van Grondelle, R. *Biophys. J.* **1996**, *70*, 669.

(46) Monshouwer, R. Unpublished results.

(47) Koepke, J.; Hu, X.; Muenke, C.; Schulten, K.; Michel, H. Technical Report UIUC-BI-TB-96-02, Beckman Institute, Urbana, IL, 1996.

(48) Kennis, J. T. M.; Streltsov, A. M.; Aartsma, T. J.; Nozawa, T.; Amesz, J. *J. Phys. Chem.* **1996**, *100*, 2438.

JP960883+